

Article

Symmetry in Recognition of Supramolecular Synthons—Competition between Hydrogen Bonding and Coordination Bond in Multinuclear Cu^{II}-4f Complexes with Bicompartamental Schiff Base Ligand

Barbara Mirosław ^{1,*} , Dariusz Osypiuk ² , Beata Cristóvão ² and Halina Głuchowska ²¹ Department of Crystallography, Faculty of Chemistry, Maria Curie-Skłodowska University, Maria Curie-Skłodowska sq. 3, 20-031 Lublin, Poland² Department of General and Coordination Chemistry, Faculty of Chemistry, Maria Curie-Skłodowska University, Maria Curie-Skłodowska sq. 2, 20-031 Lublin, Poland;

dariusz.osypiuk@poczta.umcs.lublin.pl (D.O.); beata.cristovao@poczta.umcs.lublin.pl (B.C.);

halina.gluchowska@poczta.umcs.lublin.pl (H.G.)

* Correspondence: barbara.miroslaw@poczta.umcs.lublin.pl; Tel.: +48-81-537-55-82

Received: 9 March 2019; Accepted: 27 March 2019; Published: 2 April 2019



Abstract: Classic Cu–O coordination bonds in **1** or elongated semi-coordination ones in **2** and **3** were applied to construct Cu^{II}-4f complexes composed of trinuclear subunits linked through μ -NO₃[−] ions with formulae given as [Cu₂Tm(H₂tehy)₂]₂(NO₃)₆·H₂O, (**1**), {[Cu₂Ho(H₂tehy)₂(NO₃)₂][Cu₂Ho(H₂tehy)₂(H₂O)₂]}(NO₃)₄·2H₂O, (**2**), and {[Cu₂Er(H₂tehy)₂(H₂O)]₂[(Cu₂Er(H₂tehy)₂(NO₃)₂)](NO₃)₁₀·2H₂O·4CH₃OH, (**3**), where H₂tehy = C₁₉H₂₀N₂O₄ is a tetrahydroxy Schiff base ligand. Topological analysis showed that the same characteristic motif of coordination accompanied by hydrogen bonds involving the uncoordinated nitrate oxygen atom and ligand's phenoxy O atoms is responsible for linking trinuclear subunits into a hexanuclear one as well as for bridging the hexanuclear coordination units in **3** into a 1D supramolecular polymer, with the Cu–O distance being 3.19(1) Å, much longer than the limit of a semi-coordination bond (3.07 Å). The Cambridge Structural Database was used to discuss issues of crystallographic criteria (distance and angular preferences) for the assessment of the stabilizing or destabilizing effect of hydrogen bonding on coordination. The presented results show that the symmetrically repeated arrangement of molecules may provide a useful tool for identifying higher order non-covalently bonded supramolecular aggregates. The complexes **1–3** have been characterized by X-ray diffraction, FTIR, and thermal analysis. The magnetic studies indicated the ferromagnetic interaction between Cu^{II} and Ho^{III} ions.

Keywords: semi-coordination bond; Schiff base; 3d-4f complex; Jahn-Teller distortion; hydrogen bond assisted coordination bond

1. Introduction

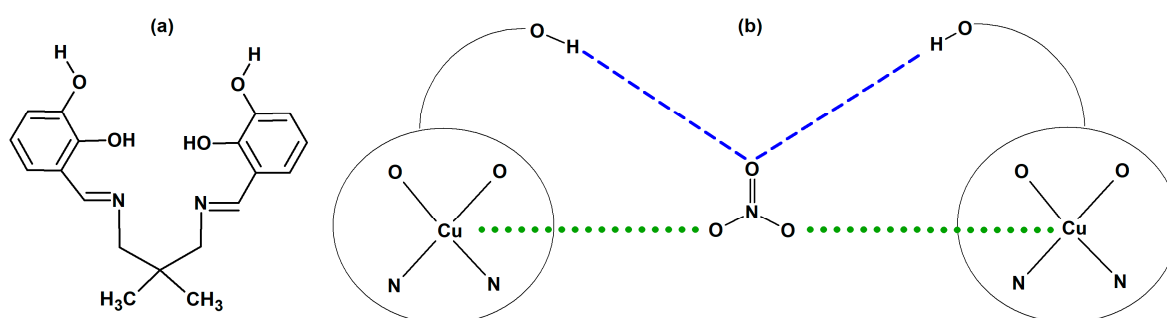
Symmetry and asymmetry are the fundamental features of matter in solids and liquids that help in the understanding of many physical phenomena and chemical reactions. Symmetry is often a useful clue for the recognition of supramolecular synthons.

The application of non-covalent interactions in crystal engineering is a thoroughly studied research area, among them hydrogen bonds [1–7], halogen bonds [8–10], dipole ··· dipole [11–14], and stacking [15–20] interactions should be mentioned. Such non-covalent interactions provide directional and stabilizing contacts that can be used successfully in the design of coordination compounds [21]. Additionally, there are also reports showing that hydrogen bonding can act as a pathway for magnetic interaction between metal ions [1,22–26].

The coordination sphere plasticity for hexacoordinated copper(II) ions is known as the Jahn–Teller effect. This distortion from ideal symmetry usually exhibits as an elongation of two axial bonds in the tetragonal bipyramid polyhedron of the complex. The Jahn–Teller deformations are believed to be stabilized in the solid state by, e.g., hydrogen bonds. The observed crystal elongation has led to the introduction of a term of a “semi-coordination bond” by Brown et al. in 1967 [27]. The theoretical studies performed by Valach et al. resulted in the calculation of the limit of a semi-coordination bond being of 3.07 or 3.04 Å for the Cu–O bond located at the elongated out-of-plane axis [28,29]. Valach also found that transition from the bonded to non-bonded state in the elongated metal–ligand direction occurs discontinuously [28].

There are some interesting reports on semi-coordinated bonds found in crystal structures of Cu^{II} cations staying within this Cu–O distance limits [29–32]. The strength of metal–ligand bonds depends on the bond length [33]. However, Nelyubina et al. proved that even very long and weak interatomic contacts (Cu ··· O 3.6 Å, 0.5 kcal/mol) may mediate magnetic super-exchange pathways [34]. On the other hand, non-covalent interactions have proved to be effective in the design of supramolecular polymers of exceptional properties [35–38].

The nitrate anion is often used in crystal engineering as a counterion since it has three oxygen atoms ready to form both coordinative and/or hydrogen bonds. However, the NO₃[−] anion generally links the neighboring copper centers by two oxygen donors independently [24]. The hydrogen bonds are usually formed with the non-coordinated nitrate oxygen. A recurrent structural motif based on nitrate ions being the interplay between a coordination or semi-coordination bond and bifurcated hydrogen bonds has been found in the presented structures 1–3 ([Cu₂Tm(H₂tehy)₂]₂(NO₃)₆·H₂O, (1), {[Cu₂Ho(H₂tehy)₂(NO₃)₂][Cu₂Ho(H₂tehy)₂(H₂O)₂]}(NO₃)₄·2H₂O, (2), and {[Cu₂Er(H₂tehy)₂(H₂O)]₂[(Cu₂Er(H₂tehy)₂(NO₃)₂)](NO₃)₁₀·2H₂O·4CH₃OH, (3), where **H₂tehy** = C₁₉H₂₀N₂O₄ is a doubly deprotonated tetrahydroxy Schiff base ligand and in previously reported ones [39,40] (Scheme 1). The topologically analogous supramolecular arrangement has been found in 3, but this time linking not only the trinuclear subunits into hexanuclear ones but also the hexanuclear ones into a linear supramolecular aggregate, with a much longer Cu ··· O_{nitrate} distance (3.19(1) Å) which is above the limit of a semi-coordination bond (3.07 Å) [28] but still shorter than the distance where a very weak interaction has been reported by Nelyubina et al. (3.6 Å) [34].



Scheme 1. (a) Structure of **H₄tehy** ligand and (b) a building motif found in 1–3; green dotted lines—out-of-plane Cu–O semi-coordination bonds at the apical positions; blue dashed lines—hydrogen bonds.

The series of Cu^{II}-4f complexes presented here formed by a tetrahydroxy compartmental Schiff base ligand **H₄tehy** (where **H₄tehy** = C₁₉H₂₂N₂O₄) and nitrate anions offers an interesting object to study the influence of hydrogen bonding on the coordination and formation of a supramolecular network.

We present here the synthesis, crystal structure, FTIR spectra, and thermal and magnetic properties of complexes 1–3 where topological similarities are discussed in terms of crystallographic distance limit of a Cu–O semi-coordination bond and the cooperative or competitive nature of coexisting coordination and hydrogen bonds.

2. Materials and Methods

2.1. Materials

Starting materials: 2,3-dihydroxybenzaldehyde, 2,2-dimethyl-1,3-propanediamine, $\text{Cu}(\text{CH}_3\text{COO})_2 \cdot \text{H}_2\text{O}$, $\text{Ho}(\text{NO}_3)_3 \cdot 5\text{H}_2\text{O}$, $\text{Er}(\text{NO}_3)_3 \cdot 5\text{H}_2\text{O}$, $\text{Tm}(\text{NO}_3)_3 \cdot 5\text{H}_2\text{O}$, and CH_3OH were purchased from commercially available sources (Sigma Aldrich) and were used without further purification. The Schiff base ligand 3-[[3-[(2,3-dihydroxyphenyl)methylideneamino]-2,2-dimethylpropyl]iminomethyl]benzene-1,2-diol (**H₂tehy**); $\text{C}_{19}\text{H}_{22}\text{N}_2\text{O}_4$) was prepared as described in the literature [41,42].

2.2. Synthesis of Complexes

The heteronuclear compounds **1–3** were synthesized as follows: To 30 mL of methanolic solution of 0.1368 g Schiff base ligand (0.4 mmol) was added dropwise 10 mL of methanolic solution of 0.0799 g $\text{Cu}(\text{CH}_3\text{COO})_2 \cdot \text{H}_2\text{O}$ (0.4 mmol,) giving a green mixture. After 30 minutes the freshly prepared solution (5 mL) of $\text{Ho}(\text{NO}_3)_3 \cdot 5\text{H}_2\text{O}$ (0.2 mmol, 0.0882 g), $\text{Er}(\text{NO}_3)_3 \cdot 5\text{H}_2\text{O}$ (0.2 mmol, 0.0887 g) or $\text{Tm}(\text{NO}_3)_3 \cdot 5\text{H}_2\text{O}$ (0.2 mmol, 0.0890 g) was slowly added to the constantly stirred suspension. The resulting deep green solution was stirred for another 30 min. A small amount of precipitate was filtered off, and the reaction mixture was left undisturbed at 4 °C. Slow evaporation yielded green crystals suitable for X-ray crystal structure analysis.

$[\text{Cu}_2\text{Tm}(\text{H}_2\text{tehy})_2]_2(\text{NO}_3)_6 \cdot \text{H}_2\text{O}$ (**1**): empirical formula $\text{C}_{76}\text{H}_{82}\text{N}_{14}\text{O}_{35}\text{Cu}_4\text{Tm}_2$, molecular weight 2343.57 g/mol. Yield 42%. Analytical data (%), Calcd: C, 38.95; H, 3.53; N, 8.37; Cu, 10.85; Tm, 14.42. Found: C, 38.50; H, 3.20; N, 8.40; Cu, 10.40; Tm, 14.00.

$\{[\text{Cu}_2\text{Ho}(\text{H}_2\text{tehy})_2(\text{NO}_3)_2][\text{Cu}_2\text{Ho}(\text{H}_2\text{tehy})_2(\text{H}_2\text{O})_2]\}(\text{NO}_3)_4 \cdot 2\text{H}_2\text{O}$ (**2**): empirical formula $\text{C}_{76}\text{H}_{88}\text{N}_{14}\text{O}_{38}\text{Cu}_4\text{Ho}_2$, molecular weight 2389.62 g/mol. Yield 38%. Analytical data (%), Calcd: C, 38.20; H, 3.71; N, 8.21; Cu, 10.64; Ho, 13.80. Found: C, 38.00; H, 3.50; N, 8.00; Cu, 10.30; Ho, 13.50.

$\{[\text{Cu}_2\text{Er}(\text{H}_2\text{tehy})_2(\text{H}_2\text{O})_2]_2([\text{Cu}_2\text{Er}(\text{H}_2\text{tehy})_2(\text{NO}_3)_2]_2)(\text{NO}_3)_{10} \cdot 2\text{H}_2\text{O} \cdot 4\text{CH}_3\text{OH}$ (**3**): empirical formula $\text{C}_{156}\text{H}_{184}\text{Cu}_8\text{Er}_4\text{N}_{28}\text{O}_{76}$, molecular weight 4844.66 g/mol. Yield 30%. Analytical data (%), Calcd: C, 38.67; H, 3.83; N, 8.10; Cu, 10.49; Er, 13.81. Found: C, 39.00; H, 3.20; N, 8.40; Cu, 10.00; Er, 13.40.

2.3. Methods

The elemental CHN analysis was performed using a CHN 2400 Perkin Elmer analyser. The contents of metals (copper, holmium, erbium, and thulium) have been determined using ED XRF spectrophotometer (Canberra–Packard). The FTIR spectra of compounds in KBr pellets were recorded in the range of 4000 to 400 cm^{-1} on the M-80 spectrophotometer (Carl Zeiss Jena). Thermal analyses of **1–3** and **H₂tehy** were conducted under air flow in the temperature range of 20 to 1000 °C (**1–3**) and 20 to 700 °C (**H₂tehy**) at a heating rate of 10 °C·min⁻¹ by the thermogravimetric (TG) and differential scanning calorimetry (DSC) methods with the use of the SETSYS 16/18 analyser (Setaram). The samples of 7.72 mg (**1**), 7.88 mg (**2**), 5.76 mg (**3**) were heated in Al_2O_3 crucibles. The XRD powder diffractograms of the decomposition products were collected at room temperature on an Empyrean PANalytical automated powder diffractometer ($\text{CuK}\alpha$ radiation $\lambda = 1.54187 \text{ \AA}$) in the 2θ range of 20 to 90°. The magnetic susceptibility for finely ground crystalline samples was measured over the temperature range of 1.8 to 300 K at magnetic field 0.1 T using a Quantum Design SQUID-VSM magnetometer. The field dependences of magnetization were investigated at 2 K in the applied field up to 5 T and were corrected by subtracting the sample–holder signal and contribution χ_D estimated from Pascal's constants [43].

Diffraction intensities for **1–3** were measured on SuperNova X-ray diffractometer (with Atlas S2 CCD detector and the mirror-monochromatized $\text{CuK}\alpha$ radiation ($\lambda = 1.54184 \text{ \AA}$) at 294 K for **1** and at 120 K for **2–3**, using the ω scan technique. The CrysAlis CCD and CrysAlis Red programs [44] have been applied for data collection, cell refinement, and data reduction. The molecular models were found by direct methods using SHELXS-97 and refined on F^2 by the full-matrix least-squares using the SHELXL-97 implemented in OLEX2 [45,46]. Non-hydrogen atoms (except the disordered part of

the ligand molecule in **3** and selected nitrate and water molecules in **1–3**) were refined anisotropically. The 2,2-dimethylpropyl bridge in **3** is disordered over two positions with site occupation factors (sof's) of the major part being of 0.6. The structure of **3** has been refined in a noncentrosymmetric space group as a two-component twin with the following twin law $(-1\ 0\ 0, 0\ 1\ 0, 0\ 0\ -1)$ (two-fold rotation about b axis with inversion twinning). The refined twin population parameter BASF (fractional contribution of twin domain calculated on batch scale factors) was 0.42. The conditions for the data collection and the crystal structure refinement parameters are shown in Table 1. The drawings were made in Mercury and Diamond software [47,48]. The experimental details and final atomic parameters for **1–3** were deposited with the Cambridge Crystallographic Data Centre as supplementary material (CCDC ID 1901698–1901700). Copies of the data can be obtained free of charge on request via www.ccdc.cam.ac.uk/data_request/cif, or by emailing data_request@ccdc.cam.ac.uk.

3. Results and Discussion

3.1. Molecular and Crystal Structure of Complexes 1–3

Compounds **1–3** were obtained by the same method of synthesis giving, however, crystal structures of different symmetry. The complexes show subtle differences in the coordination architecture and in the degree of Jahn–Teller distortion of Cu^{II} ions.

3.2. Hexanuclear Complex of **1**

Compound **1** form crystals in the monoclinic space group ($C2/c$) with half of the coordination unit being symmetrically independent (Table 1). The asymmetric part consists of a trinuclear $\text{Cu}^{\text{II}}\text{–Tm}^{\text{III}}\text{–Cu}^{\text{II}}$ core linked by a bridging nitrate anion (lying on the two-fold axis) to the other half resulting in a hexanuclear coordination entity with the Cu2–O10 coordination bond length being 2.594(5) Å (Figures 1 and 2; Tables 2 and 3). This characteristic motif is supplemented by two $\text{O4–H4} \cdots \text{O9}$ hydrogen bonds with a bifurcated acceptor O atom (Table 4). A similar characteristic arrangement of two trinuclear subunits linked by a bridging NO_3^- ion and hydrogen bonds has been discussed in structures of **2** and **3**.

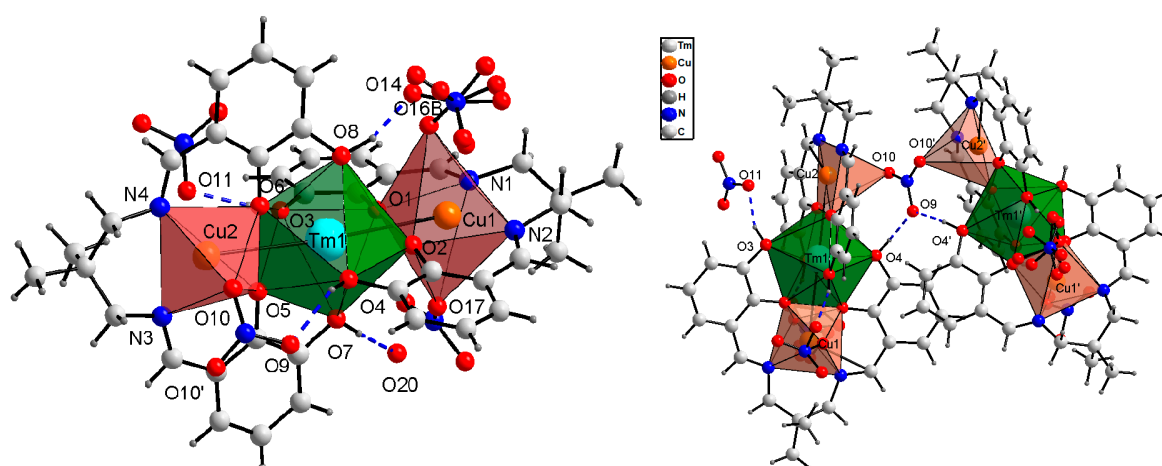


Figure 1. View at the asymmetric unit in **1** (left) and view at the hexanuclear unit repeated by a two-fold axis (right) linked by semi-coordination bond Cu2–O10 and hydrogen bonds (marked with dashed lines).

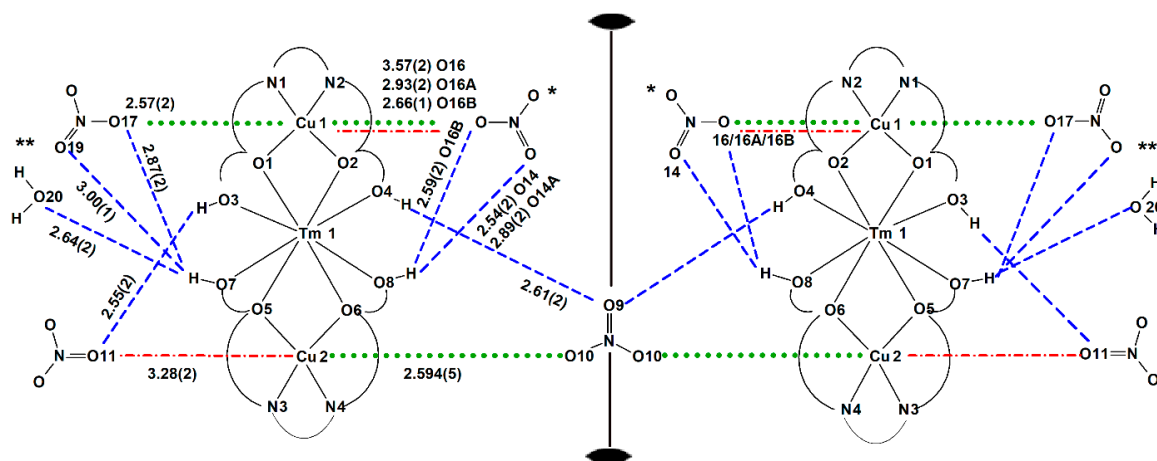


Figure 2. Scheme of coordination unit in complex **1** with Cu–O and O···O distances in angstrom (Å), the position of two-fold axis is marked, the two halves are related by a two-fold axis, green dotted lines—semi-coordination Cu–O bonds at the apical positions, red dash–dotted lines—contact behind the limit of a semi-coordination bond but topologically important, blue dashed lines—hydrogen bonds, * nitrate anion disordered other three positions (sof's 0.33), ** disorder of water and nitrate anion (sof's 0.5).

Table 1. Crystal data and structure refinement details for **1–3**.

Identification Code	1	2	3
Empirical formula	C ₇₆ H ₈₂ N ₁₄ O ₃₅ Cu ₄ Tm ₂	C ₇₆ H ₈₈ N ₁₄ O ₃₈ Cu ₄ Ho ₂	C ₁₅₆ H ₁₈₄ N ₂₈ O ₇₆ Cu ₈ Er ₄
Formula weight	2343.57	2389.62	4844.66
Temperature/K	294.1(3)	120.0(0)	120.0(1)
Crystal system	monoclinic	monoclinic	orthorhombic
Space group	C2/c	P2 ₁ /c	Pnc2
<i>a</i> /Å	26.043(1)	26.134(1)	16.8980(4)
<i>b</i> /Å	15.0653(4)	15.5412(6)	33.1478(7)
<i>c</i> /Å	22.7584(9)	21.515(1)	15.5493(3)
α /°	90	90	90
β /°	101.659(4)	94.386(5)	90
γ /°	90	90	90
Volume/Å ³	8744.9(5)	8712.5(7)	8709.6(3)
Z	4	4	2
ρ_{calc} g/cm ³	1.780	1.822	1.847
μ /mm ^{−1}	5.508	5.149	5.342
<i>F</i> (000)	4680.0	4784.0	4856.0
Crystal size/mm ³	0.22 × 0.2 × 0.15	0.2 × 0.1 × 0.05	0.25 × 0.08 × 0.02
Radiation	CuK α (λ = 1.54184)	CuK α (λ = 1.54184)	CuK α (λ = 1.54184)
2 θ range for data collection/°	6.814 to 135.366	6.622 to 135.364	7.472 to 153.146
Index ranges	−31 ≤ <i>h</i> ≤ 25, −17 ≤ <i>k</i> ≤ 18, −27 ≤ <i>l</i> ≤ 26	−31 ≤ <i>h</i> ≤ 31, −18 ≤ <i>k</i> ≤ 14, −25 ≤ <i>l</i> ≤ 25	−21 ≤ <i>h</i> ≤ 18, −30 ≤ <i>k</i> ≤ 41, −19 ≤ <i>l</i> ≤ 18
Reflections collected	29701	60265	65209
Independent reflections	7897 [<i>R</i> _{int} = 0.0434, <i>R</i> _{sigma} = 0.0366]	15748 [<i>R</i> _{int} = 0.1026, <i>R</i> _{sigma} = 0.0951]	17487 [<i>R</i> _{int} = 0.0537, <i>R</i> _{sigma} = 0.0509]
Data/restraints/parameters	7897/40/586	15748/36/1218	17487/37/1220
Goodness-of-fit on <i>F</i> ²	1.058	0.984	1.033
Final <i>R</i> indexes [<i>I</i> ≥ 2 σ (<i>I</i>)]	<i>R</i> ₁ = 0.0596, <i>wR</i> ₂ = 0.1696	<i>R</i> ₁ = 0.0599, <i>wR</i> ₂ = 0.1498	<i>R</i> ₁ = 0.0425, <i>wR</i> ₂ = 0.1076
Final <i>R</i> indexes [all data]	<i>R</i> ₁ = 0.0727, <i>wR</i> ₂ = 0.1922	<i>R</i> ₁ = 0.0978, <i>wR</i> ₂ = 0.1788	<i>R</i> ₁ = 0.0529, <i>wR</i> ₂ = 0.1333
Largest diff. peak/hole/e Å ^{−3}	1.33/−1.13	1.36/−1.33	1.12/−1.32
Flack parameter	—	—	0.001(5)
CCDC No.	1901698	1901699	1901700

Table 2. Selected bond lengths and Cu···O contacts in angstrom (Å) for crystals 1–3.

1		2		3	
Tm1–Cu1	3.463(1)	Ho1–Cu1	3.455(1)	Er1–Cu1	3.443(2)
Tm1–Cu2	3.4636(9)	Ho1–Cu2	3.454(1)	Er1–Cu2	3.473(2)
Tm1–O1	2.280(5)	Ho1–O1	2.288(4)	Er1–O1	2.296(7)
Tm1–O2	2.317(4)	Ho1–O2	2.298(4)	Er1–O2	2.283(6)
Tm1–O3	2.289(5)	Ho1–O3	2.408(5)	Er1–O3	2.377(7)
Tm1–O4	2.377(5)	Ho1–O4	2.355(4)	Er1–O4	2.363(7)
Tm1–O5	2.291(5)	Ho1–O5	2.294(5)	Er1–O5	2.297(7)
Tm1–O6	2.306(4)	Ho1–O6	2.300(5)	Er1–O6	2.324(7)
Tm1–O7	2.326(6)	Ho1–O7	2.379(5)	Er1–O7	2.251(7)
Tm1–O8	2.368(5)	Ho1–O8	2.348(5)	Er1–O8	2.412(6)
Cu1–O1	1.934(5)	Ho2–Cu3	3.513(1)	Er2–Cu3	3.474(2)
Cu1–O2	1.941(4)	Ho2–Cu4	3.491(1)	Er2–Cu4	3.449(2)
Cu1–N1	1.983(5)	Ho2–O9	2.354(5)	Er2–O9	2.301(7)
Cu1–N2	1.987(6)	Ho2–O10	2.321(5)	Er2–O10	2.312(7)
Cu1–O17	2.57(2)	Ho2–O11	2.421(5)	Er2–O11	2.355(7)
Cu1···O16	3.57(2)	Ho2–O12	2.399(5)	Er2–O12	2.388(7)
Cu1–O16A	2.93(2)	Ho2–O13	2.359(5)	Er2–O13	2.286(7)
Cu1–O16B	2.66(1)	Ho2–O14	2.335(5)	Er2–O14	2.314(6)
Cu1–O17	2.57(2)	Ho2–O15	2.446(6)	Er2–O15	2.238(7)
Cu2–O5	1.930(5)	Ho2–O16	2.481(5)	Er2–O16	2.417(7)
Cu2–O6	1.935(4)	Ho2–O38A	2.44(1)	Cu1–O1	1.959(8)
Cu2–N3	1.977(5)	Ho2–O38	2.372(9)	Cu1–O2	1.939(7)
Cu2–N4	1.975(5)	Cu1–O1	1.949(5)	Cu1–N1	1.99(1)
Cu2–O10	2.594(5)	Cu1–O2	1.953(5)	Cu1–N2	1.99(1)
Cu2···O11	3.28(2)	Cu1–N1	1.982(6)	Cu1–O17	2.29(1)
		Cu1–N2	1.979(6)	Cu1–O30	2.83(1)
		Cu1–O32	2.497(6)	Cu2–O5	1.90(1)
		Cu1···O35	3.89(1)	Cu2–O6	1.959(7)
		Cu2–O5	1.933(5)	Cu2–N3	1.995(9)
		Cu2–O6	1.939(5)	Cu2–N4	1.948(9)
		Cu2–N3	1.967(6)	Cu2–O37	2.908(9)
		Cu2–N4	1.965(6)	Cu2–O18	3.19(1)*
		Cu2–O24	2.488(5)	Cu3–O9	1.922(7)
		Cu2···O26	3.356(7)	Cu3–O10	1.952(7)
		Cu3–O9	1.933(5)	Cu3–O21	2.44(1)
		Cu3–O10	1.960(5)	Cu3–N7	1.977(9)
		Cu3–N5	1.989(6)	Cu3–N8	1.962(9)
		Cu3–N6	1.972(6)	Cu3–O21	2.44(1)
		Cu3–O25	3.031(5)	Cu3···O38	3.613(8)
		Cu3–O37	2.478(8)	Cu4–O13	1.915(7)
		Cu4–O13	1.953(5)	Cu4–O14	1.958(7)
		Cu4–O14	1.936(5)	Cu4–N5	1.969(9)
		Cu4–N7	1.972(6)	Cu4–N6	1.965(9)
		Cu4–N8	1.972(6)	Cu4–O27	2.565(7)
		Cu4–O18	2.565(6)	Cu4–O20	3.01(1)
		Cu4–O22	2.603(5)		

* distance above the limit of 3.07 Å for semi-coordination bond but recognized as a semi-coordinative assisted by hydrogen bonding.

Table 3. Selected bond angles in degrees for 1–3.

1		2		3	
Cu1–O1–Tm1	110.3(2)	Cu1–O1–Ho1	109.0(2)	Cu1–O1–Er1	107.8(3)
Cu1–O2–Tm1	108.5(2)	Cu1–O2–Ho1	108.5(2)	Cu1–O2–Er1	109.0(3)
Cu2–O5–Tm1	110.0(2)	Cu2–O5–Ho1	109.3(2)	Cu2–O5–Er1	111.3(3)
Cu2–O6–Tm1	109.2(2)	Cu2–O6–Ho1	108.8(2)	Cu2–O6–Er1	108.1(3)
Cu1–Tm1–Cu2	175.6(1)	Cu3–O9–Ho2	109.7(2)	Cu3–O9–Er2	109.2(3)
		Cu3–O10–Ho2	110.0(2)	Cu3–O10–Er2	107.7(3)
		Cu4–O13–Ho2	107.7(2)	Cu4–O13–Er2	111.3(3)
		Cu4–O14–Ho2	109.3(2)	Cu4–O14–Er2	108.6(3)
		Cu1–Ho1–Cu2	170.5(1)	Cu1–Er1–Cu2	174.3(1)
		Cu3–Ho2–Cu4	177.1(1)	Cu3–Er2–Cu4	171.3(1)

The smaller N₂O₂ compartments are occupied by Cu^{II} cations. Cu1 ion has the coordination number of five or six because one of the monodentate NO₃[−] anions is disordered over three positions. The Cu1···O16/O16A/O16B distance varies from 2.66(1) to 3.57(1) Å (Table 2), which differentiates the character of the interatomic contact (semi-coordination or non-bonding). The nitrate ion may be bonded directly to Cu1 cation by a coordinative bond, or it can act as a hydrogen bond acceptor in O8–H8···O14 interaction (Figures 1 and 2; Table 4). Cu2 cation is penta-coordinated. The apical position of the polyhedron is occupied by a bridging nitrate ion with Cu2–O10 bonds being of 2.594(5) Å. The Cu2 ion has also a long contact, above the limit of a semi-coordination bond (Cu2···O11 3.28(2) Å), to a nitrate anion hydrogen bonded through the same O11 atom to the phenoxy group (O3–H3···O11 interaction). The Tm^{III} ion is octa-coordinated by two O₄ cavities of the perpendicularly oriented Schiff base ligands. In the crystal structure, there is only one uncoordinated solvent molecule—water linked strongly by a hydrogen bond to the H₂tehy ligand (Table 4).

Table 4. Selected hydrogen bonds for 1–3.

Crystal	D–H···A	D–H	H···A	D···A	∠D–H···A
1	O3–H3···O11	0.87	1.76	2.55(2)	150
	O4–H4···O9	0.87	1.88	2.614(6)	143
	O7–H7···O17	0.87	2.26	2.87(2)	128
	O7–H7···O19	0.87	2.26	3.00(1)	144
	O7–H7···O20	0.87	1.80	2.64(2)	165
	O8–H8···O14	0.87	1.61	2.54(2)	161
	O8–H8···O14A	0.87	2.02	2.89(2)	150
	O8–H8···O16B	0.87	1.67	2.59(2)	157
2	O3–H3···O23	0.86	1.79	2.628(7)	167
	O4–H4···O26	0.86	1.69	2.535(8)	167
	O7–H7···O32	0.86	1.75	2.545(8)	154
	O8–H8···O35	0.86	1.74	2.544(9)	158
	O35–H35A···O36 ⁱ	0.86	2.22	2.819(16)	127
	O11–H11···O20	0.86	1.76	2.592(9)	167
	O12–H12···O17	0.86	1.76	2.587(8)	166
	O15–H15···O29	0.86	1.80	2.621(10)	163
	O16–H16···O23	0.86	1.97	2.723(8)	148
	O38A–H38A···O37 ⁱⁱ	0.89	2.23	3.04(1)	152
	O38–H38C···O22 ⁱⁱ	0.89	2.64	3.14(1)	118
	O37–H37A···O29	0.85	2.04	2.719(15)	135
	O37–H37B···O30 ⁱⁱⁱ	0.85	2.03	2.825(15)	154
	O36–H36B···O35 ⁱ	0.89	2.49	2.819(16)	103
	O35–H35A···O26 ^{iv}	0.85	2.018	2.83(1)	159.6
3	O3–H3···O19	0.86	1.78	2.61(1)	162
	O4–H4···O37	0.86	1.73	2.55(1)	158
	O7–H7···O17	0.86	1.85	2.66(1)	134
	O8–H8···O29	0.86	1.81	2.641(8)	164
	O11–H11···O19	0.86	2.50	3.10(1)	127
	O11–H11···O20	0.86	1.79	2.60(1)	159
	O12–H12···O28	0.86	1.79	2.617(9)	160
	O15–H15···O38	0.86	1.79	2.66(1)	163
	O16–H16···O23	0.86	1.91	2.72(1)	158
	O17A–H17A···O38	0.86	1.95	2.76(1)	156
	O39–H39A···O18	0.86	2.31	2.96(1)	131
	O37–H37···O34	0.84	1.80	2.63(1)	171

Symmetry codes: ⁱ x, 1.5 – y, –0.5 + z; ⁱⁱ 1 – x, –y, –z; ⁱⁱⁱ 2 – x, –y, 1 – z; ^{iv} x, 0.5 – y, 0.5 + z.

3.3. Dimer of Trinuclear Cores Linked by a Semi-Coordination Bond in 2

The – coordination unit in the monoclinic crystal 2 (*P*2₁/*c*) is built of two symmetrically independent trinuclear Cu^{II}–Ho^{III}–Cu^{II} coordination moieties linked by a bidentate nitrate ligand into one hexanuclear entity (Figures 3 and 4). However, the distances between the O nitrate atom and Cu^{II} centers are different: 2.488(5) and 3.031(5) Å for Cu2–O24 and Cu3–O25 pairs of atoms, respectively. The first distance may be regarded as a classic coordination bond, whereas, the other one is very

long but still within the limit of a semi-coordination bond (3.07 Å). Additionally, the coordination motif is again accompanied by two bifurcated hydrogen bonds O3–H3···O23 and O16–H16···O23 to the non-coordinated nitrate O atom, similar to **1**. The hydrogen bonding seems to compete with the coordination bond causing the elongation of the Cu3–O25 distance above the conventional coordinative bond limit, but it seems to stabilize the whole motif. Because of the topological similarities between structures **1** and **2**, the Cu3–O25 bond has been recognized as a semi-coordinative one, and the structure of **2** as a hexanuclear one.

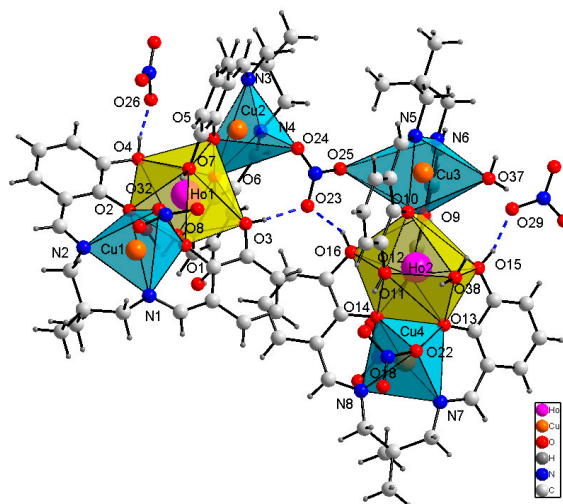


Figure 3. Coordination polyhedra and selected hydrogen bonds (dashed lines) in **2**.

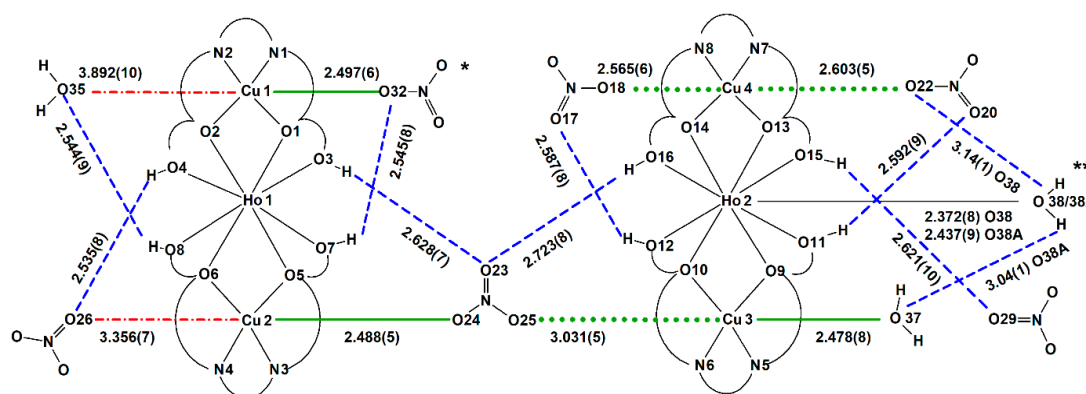


Figure 4. Scheme of coordination in complex **2** with Cu–O and O···O distances in angstrom (Å), green bold lines—coordination bonds Cu–O at the apical positions, green dotted lines—Cu–O semi-coordination bonds at the apical positions, red dash–dotted lines—contacts behind the limit of a semi-coordination bond but topologically important, blue dashed lines—hydrogen bonds, * nitrate anion disordered over two positions (sof’s 0.5); ** water molecule disordered other two positions (sof’s 0.6:0.4).

The Cu^{II} ions occupy the N₂O₂ cavities of the doubly deprotonated **H₂tehy** ligand. Cu1 and Cu2 cations have a coordination number (CN) of five. The apical position of tetragonal pyramids occupies NO₃[−] ions. The contacts between atoms Cu1···O35 (3.89(1) Å) and Cu2···O26 (3.356(7) Å) are much longer than coordinative ones. Additionally, the same nitrate O atom is involved in hydrogen bonding (Figure 4, Table 4). Cu2 is linked by the nitrate bridge to Cu3 ion. The non-bonding nitrate O23 atom accepts two bifurcated hydrogen bonds closing the characteristic building motif. Cu3 (CN = 6) supplements its coordination sphere with a water molecule (Cu3–O37 2.475(8) Å). Cu4 (CN = 6) coordinates two monodentate NO₃[−] ions. The Ho1 ion has the same coordination environment as Tm1 in **1**, whereas, Ho2 is nona-coordinated. Except for two perpendicularly located **H₂tehy** ligands,

there are two other positions which are disordered water molecules. This results in the change in conformation of the Schiff base ligands, which adopt a bent conformation instead of nearly planar as in **1**. The remaining uncoordinated nitrate anions and water molecules interact through many hydrogen bonds (Table 4).

3.4. Supramolecular Polymer Built of Hexanuclear Monomers in **3**

Compound **3** crystallizes in the orthorhombic *Pnc2* space group with two types of symmetrically independent hexanuclear coordination units composed of trinuclear subunits A and B linked by the NO_3^- ions into AA and BB entities (Figures 5 and 6).

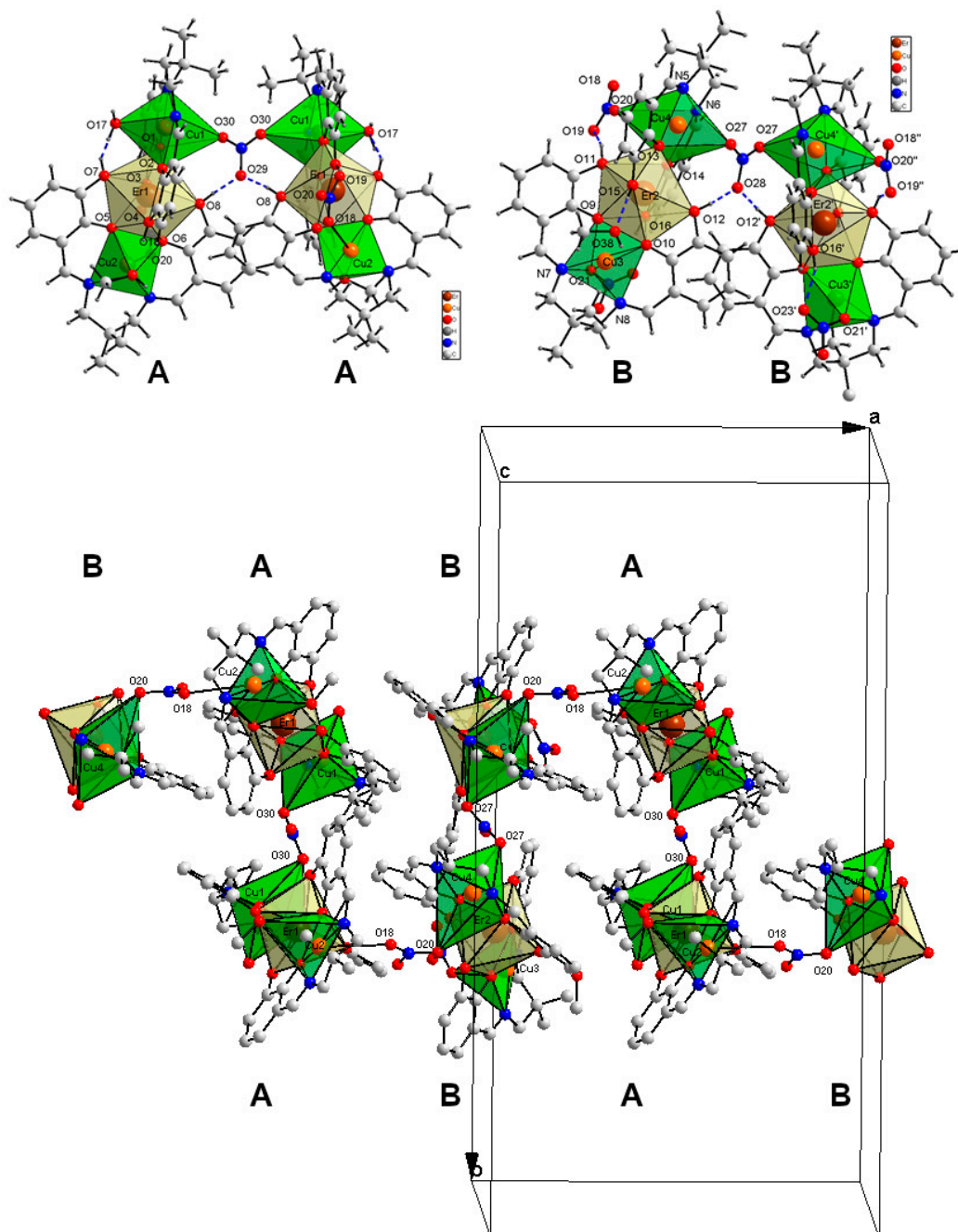


Figure 5. Hexanuclear coordination units composed of trinuclear subunits A and B in **3** (top) and the suggested supramolecular polymeric chain AA-BB-AA-BB in **3** (bottom); symmetry codes: ' $-x, 1 - y, z$; " $1 - x, 1 - y, z$.

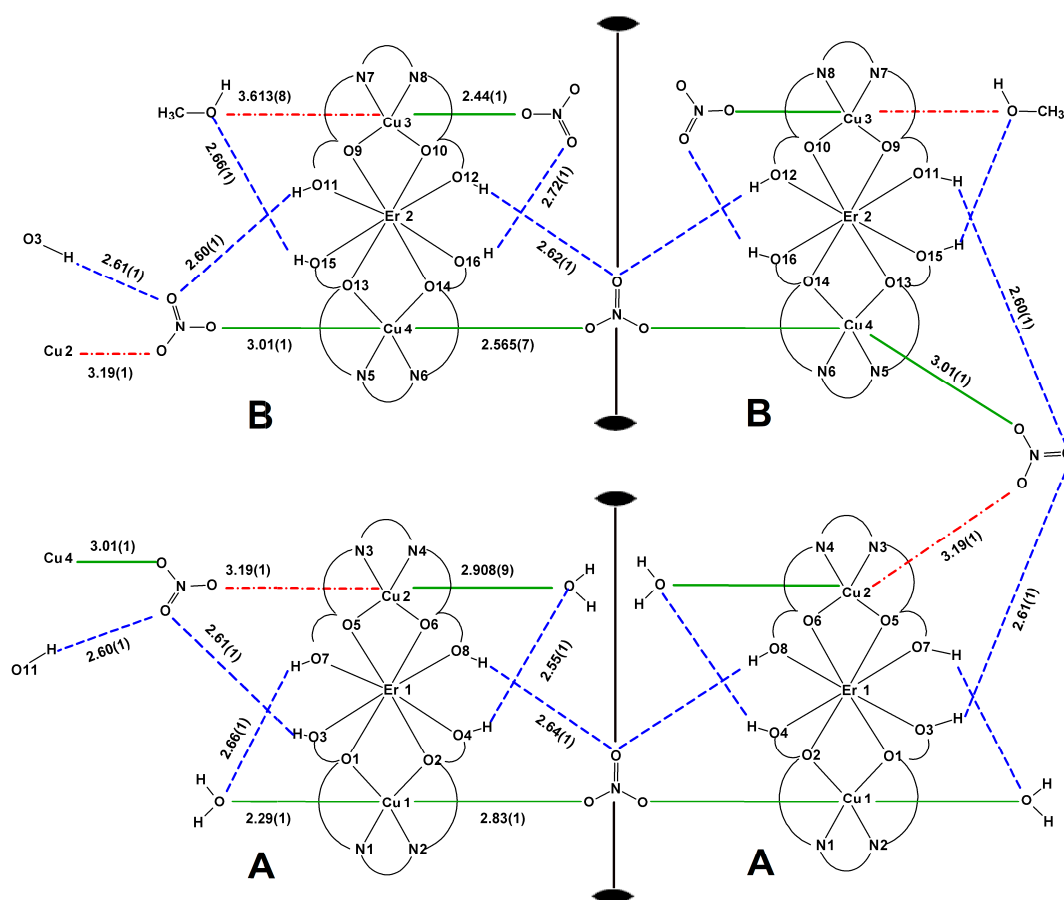


Figure 6. Scheme of coordination in complex **3** with Cu–O and O···O distances in Å, the position of two-fold axes is marked, green bold lines—coordination bonds Cu–O at the apical positions, green dotted lines—Cu–O semi-coordination bonds at the apical positions, red dash-dotted lines—contacts behind the limit of a semi-coordination bond but topologically important, blue dashed lines—hydrogen bonds.

In a topological sense, compound **3** may be regarded as a 1D supramolecular polymer AA–BB–AA–BB running as a folded chain along the *a* axis with hexanuclear entities AA and BB linked by an elongated semi-coordinative bond (Cu4–O20 3.01(1) Å) and by a long contact of the same topology but probably of a different nature of interaction (Cu2–O18 3.19(1) Å). Each of these semi-coordination bonds or contacts is accompanied by a specific array of hydrogen bonds forming the characteristic motif found in **1** and **2** (Figure 6).

The assumption of an attractive character of this long contact is based on topological similarities of the recurrent supramolecular motif found in **1–3** and on the results of studies performed by Nelyubina et al. [34]. The stabilizing effect is provided by the accompanying hydrogen bonds O3–H3···O19, O11–H11···O19, and O11–H11···O20 (Table 4), wherein it is important that the hydrogen bonding occurs through the non-coordinated O nitrate atoms. The Er^{III} cation is octa-coordinated as Tm^{III} in **1**. Cu1 (CN = 6) has H₂O molecule in the apical position and μ -NO₃[−] ion at the other apex of a tetragonal bipyramid. The nitrate anion links by a semi-coordination bond (Cu1–O30 2.83(1) Å) two related by a two-fold rotation Cu1 ions into a hexanuclear unit. The apical ligands of Cu2 ion (CN = 6) are one methanol molecule and one NO₃[−] anion with a very long Cu2–O18 contact distance (3.19(1) Å) bridging to Cu4 cation. The Cu4 (CN = 6) is linked further to a repeated by a two-fold axis to another Cu4 ion. Cu3 (CN = 5) ion coordinates one monodentate nitrate ion. The Cu3···O38 (3.613(8) Å) contact was not identified as a coordinative because of the long distance and a competitive influence of O15–H15···O38 hydrogen bond (interaction to the same O_{nitrate} atom).

3.5. The Geometric Criteria for a Semi-Coordination Bond on the Base of CSD Search

For the search of Cambridge Structural Database (CSD, ver. 5.40 Nov. 2018) the Conquest software (ver. 2.0.0.) was used, the restrictions were as follows R values <5%, no disorder, no powder structures [47]. The search for Cu···O–NO₂ distances up to 4 Å without determining the type of bonding or contact gave 1068 results. The number of occurrences of a given Cu–O distance (Figure 7) clearly confirm the Jahn–Teller distortion: 1) the first sharp peak with the maximum at *ca.* 1.9 Å corresponds to the shorter in-plane coordination bonds, 2) the next population of longer Cu–O distances has a wider range with a lower maximum at *ca.* 2.5 Å (Cu–O distance to the out-of-plane ligands). Next, the number of occurrence of Cu···O contacts seems to be nearly constant from three until *ca.* 3.5 Å, where it starts to grow with a small increase at *ca.* 3.1 Å. From the crystallographic point of view, this plot does not indicate any sharp border between coordination and semi-coordination bonding nor the sharp border of the second one.

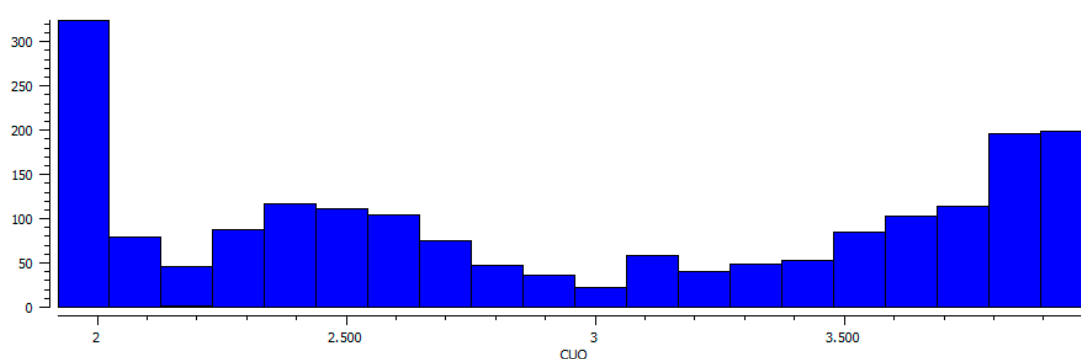


Figure 7. Distribution of Cu···O distance values up to 4 Å found in Cambridge Structural Database (CSD).

The plot of Cu···O–N(O₂) angle shows three maxima at *ca.* 7, 75, and 115° (Figure 8). The highest maximum at *ca.* 115° corresponds to the optimal orientation of oxygen lobes toward the positive charge of the Cu center in coordination bonding, the peaks at *ca.* 7 and 75° are related to the angles between Cu and the non-interacting nitrate oxygen atoms.

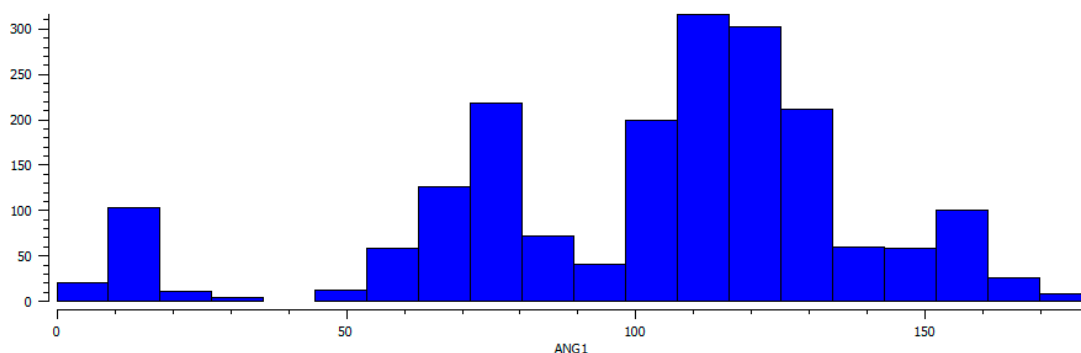


Figure 8. Distribution of Cu···O–N(O₂) angle values (ANG1 in °) found in CSD.

It shows a clear directional preference in the orientation of nitrate ions toward the Cu metal centers (semi-coordination Cu···O–N(O₂) angle in the range of *ca.* 100 to 140°). It is even more pronounced at the scatter plot of Cu···O–N(O₂) angle *vs* Cu···O distance values (Figure 9). The directionality is sustained until *ca.* 3.65 Å and only above this distance limit does the distribution of Cu···O–N(O₂) valence angles start to be more random.

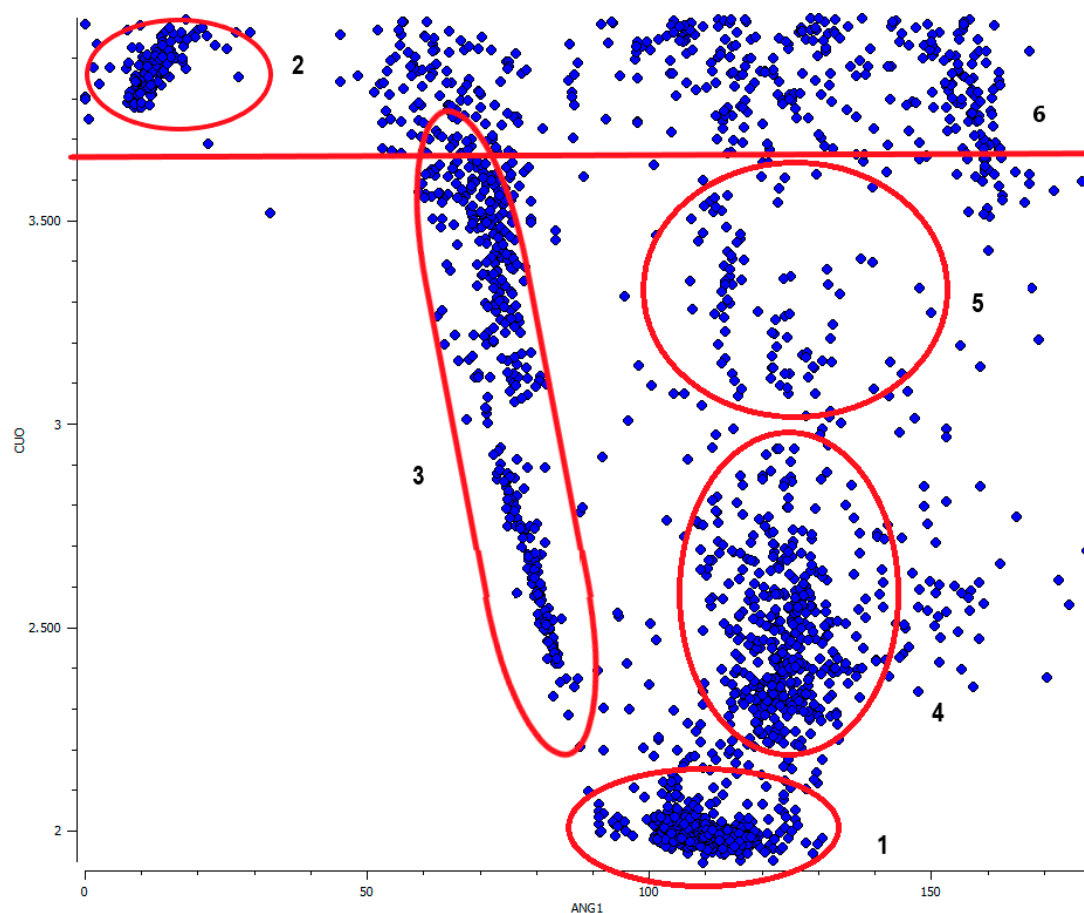


Figure 9. Scatter plot of Cu \cdots O–N(O₂) angle (ANG1 in °) vs Cu \cdots O distance (CUO in Å) up to 4 Å with marked six regions described in the text.

At the scatter plot (Figure 9) six groups of data can be distinguished: (1) the group of classic coordination bond to the in-plane ligands with short Cu \cdots O distance (up to *ca.* 2.2 Å) and Cu \cdots O–N(O₂) angle being in the range of 90 to 130°; (2) and (3) are clearly distinctive groups with low valence angles 5 to 10° and 60 to 90° and ranges of Cu \cdots O distances above 3.65 Å and 2.3–3.7 Å, respectively. They correspond to the non-bonding contacts to the neighborly located oxygen atoms within the same coordinated NO₃[−] molecule; (4) the elongated coordination or semi-coordination bond to the out-of-plane ligands (Cu–O bond *ca.* 2.3–3 Å, Cu \cdots O–N(O₂) angle *ca.* 110–140°); (5) the extended area for very long interactions of a different character but still with a high degree of directionality (Cu \cdots O distance *ca.* 3–3.65 Å, Cu \cdots O–N(O₂) angle *ca.* 100–150°), could be probably hydrogen bond assisted coordination bonds. Additionally, in this group, if the regarded Cu \cdots O–N(O₂) contact was not included as a coordination, nearly all of the copper(II) centers were tetra- or penta-coordinated and the nitrate anion was located at the “free” non-coordinated side of the central ion closing, at least in a topological sense, the coordination sphere of copper; (6) Group of contacts above 3.65 Å showing no specific directional preferences. A similar distribution of Cu–O distances and Cu–O–X(O₂) angles was observed in the group of other oxo complexes, where X was C or N; 7226 data, Figure S1 in Supplementary Materials).

3.6. Infrared Spectra

The obtained Cu^{II}–4f complexes show similar FTIR spectral features (Figure 10 and Figures S2–S4). A strong band at 1620 cm^{−1} from ν (C=N_{imine}) is red-shifted by 20 cm^{−1} in comparison to the free H₄tehy ligand indicating a decrease of the C=N bond order because of the formation of the coordination bond to the copper(II). The broad band with a maximum at *ca.* 3400 cm^{−1} comes from

$\nu(\text{O-H})$ stretching vibrations of coordinated and/or solvated water/methanol molecules and from the undeprotonated hydroxyl groups of the H_4tehy ligand. The strong phenolic $\nu(\text{C-O})$ stretching vibration band was observed at 1240 cm^{-1} for free H_4tehy ligand, whereas, in complexes there was a doublet with peaks at 1252 and 1220 cm^{-1} , confirming the coordination through these groups [49–53].

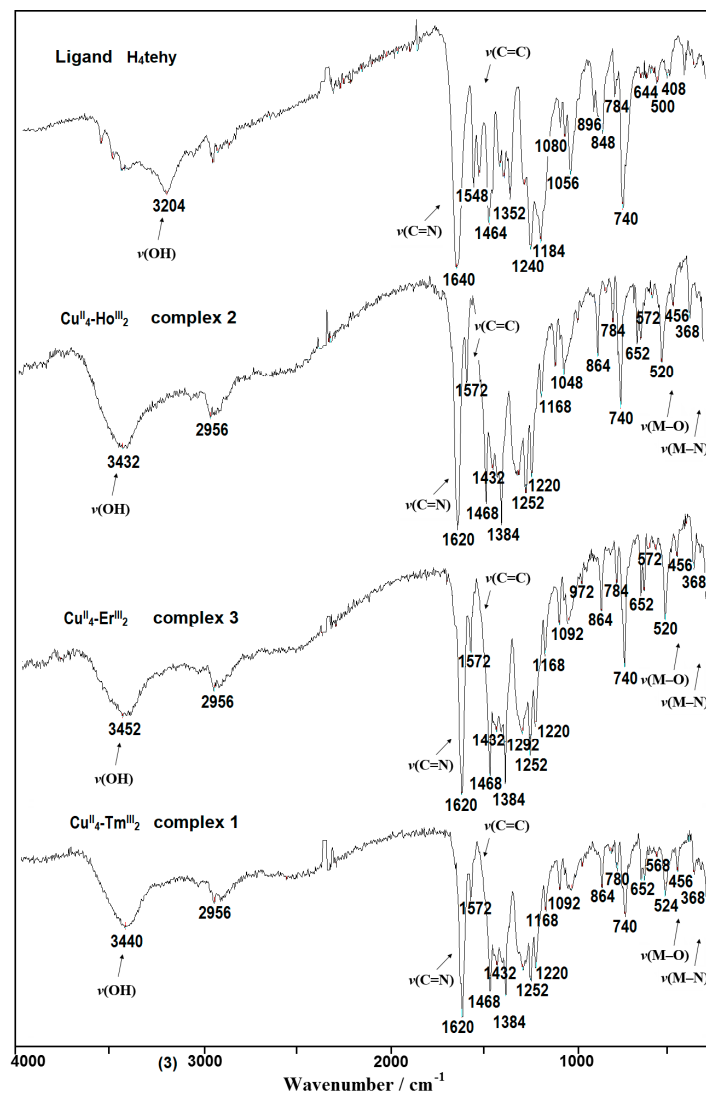


Figure 10. FTIR spectra of the ligand H_4tehy and its complexes 1–3.

3.7. Thermal Properties

The TG, DTG, and DSC curves of 1–3 (Figure 11 and Figures S5–S7) show that the $\text{Cu}^{\text{II}}\text{-}4f$ compounds are stable at room temperature. During heating to *ca.* $100\text{ }^\circ\text{C}$ the complexes 1–3 desolvate with a mass loss found 1.20% (1), 2.00% (2), 3.60% (3); calculated 0.80% (1), 1.50% (2), 3.40% (3).

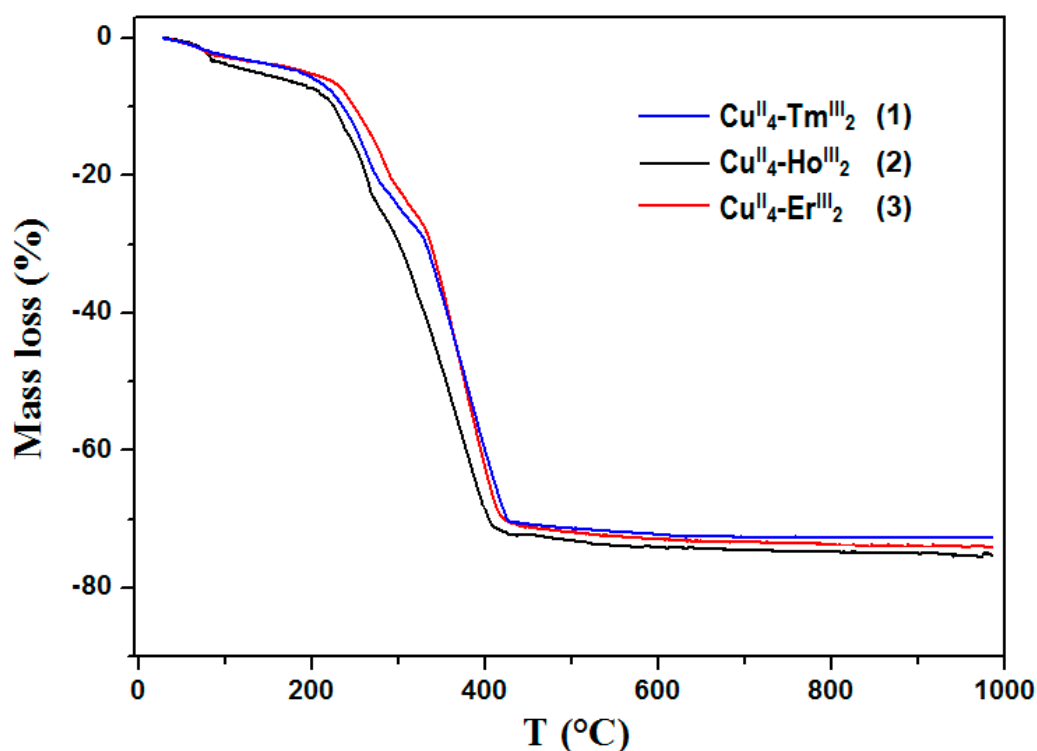


Figure 11. Thermogravimetric (TG) curves of complexes 1–3 in air.

The DSC curves indicate a small endothermic effect. The decomposition process of the $\text{Cu}^{\text{II}}\text{-4}f$ compounds was intricate, and the intermediate solid products were hard to distinguish. The final decomposition products of 1–3 were mixtures of metal oxides CuO and $\text{Ho}_2\text{O}_3/\text{Er}_2\text{O}_3/\text{Tm}_2\text{O}_3$ (calculated from TG curves and verified experimentally by powder XRD patterns (Figure S8)). The calculated TG curves percentages (29.40% (1), 31.00% (2), 31.50% (3)) coincided with the theoretical values 30.00% (1), 28.90% (2), 30.00% (3).

3.8. Magnetic Properties

The plots of temperature-dependent molar susceptibility ($\chi_{\text{M}}T$ versus T) were shown in Figure 12, where χ_{M} is the molar magnetic susceptibility, and T is the absolute temperature. The magnetic properties of the complexes result from the interplay between three factors: the $\text{Cu}^{\text{II}} \cdots \text{Cu}^{\text{II}}$ and $\text{Cu}^{\text{II}}\text{-Ln}^{\text{III}}$ interactions, as well as the thermal population of the Stark components of the lanthanide(III) ions. The $\chi_{\text{M}}T$ values of the complexes studied at room temperature were calculated theoretically by the Equation (1) assuming four Cu^{II} and two magnetically isolated Ln^{III} ions.

$$\chi_{\text{M}}T = \left(\left(N\beta^2/3k \right) \left[4g_{\text{Cu}}^2 S_{\text{Cu}}(S_{\text{Cu}} + 1) + 2g_{\text{Ln}}^2 J_{\text{Ln}}(J_{\text{Ln}} + 1) \right] \right) \quad (1)$$

where N is Avogadro constant, β is the Bohr magneton, and k is Boltzman's constant. In this equation g_{Ln} is the g factor of the ground J terms of Ln^{III} and is expressed as in Equation (2):

$$g_{\text{Ln}} = \frac{3}{2} + \frac{S(S+1) - L(L+1)}{2J(J+1)} \quad (2)$$

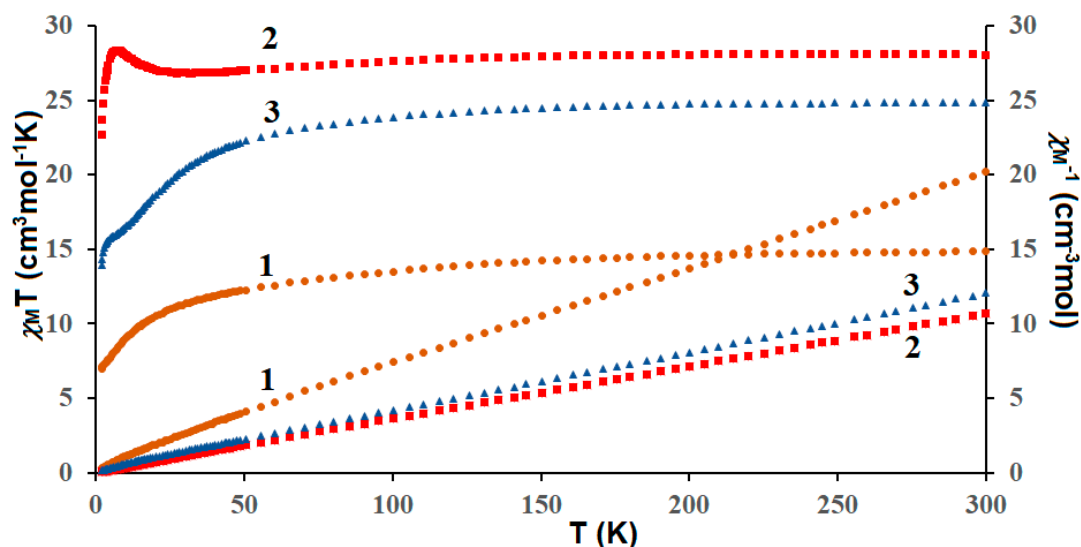


Figure 12. Temperature dependence of experimental $\chi_M T$ and χ_M^{-1} versus T for $\text{Cu}^{\text{II}}-4f$ complexes 1–3.

In $\text{Cu}^{\text{II}}_4\text{-Tm}^{\text{III}}_2$ (1) complex the $\chi_M T$ value of $14.85 \text{ cm}^3 \text{Kmol}^{-1}$ observed at 300 K corresponds to the value of $15.80 \text{ cm}^3 \text{Kmol}^{-1}$ expected for two Tm^{III} ($^3\text{H}_6$, $S = 1$, $L = 5$, $J = 6$, $g = 3/2$) and four Cu^{II} ($S = 1/2$, $g = 2$) magnetically isolated ions. This value steadily decreased as T was lowered to reach $6.99 \text{ cm}^3 \text{Kmol}^{-1}$ at 1.8 K. For $\text{Cu}^{\text{II}}_4\text{-Ho}^{\text{III}}_2$ (2) the $\chi_M T$ value experimentally determined at 300 K ($28.04 \text{ cm}^3 \text{Kmol}^{-1}$) is slightly lower than the value of $29.63 \text{ cm}^3 \text{Kmol}^{-1}$ expected for two Ho^{III} ($^5\text{I}_8$, $J = 8$, $L = 6$, $S = 2$, $g = 5/4$) and four Cu^{II} ($S = 1/2$, $g = 2$) noninteracting metal ions. With the lowering of the temperature the $\chi_M T$ remained constant until 120 K, then it decreased to $27.00 \text{ cm}^3 \text{Kmol}^{-1}$ at 19 K and next increased to reach a value of $28.48 \text{ cm}^3 \text{Kmol}^{-1}$ at 6.6 K. Finally, it showed a small decrease to $22.07 \text{ cm}^3 \text{Kmol}^{-1}$ at 1.8 K. For the compound $\text{Cu}_4^{\text{II}}\text{-Er}_2^{\text{III}}$ (3) the experimental value of $\chi_M T$ at room temperature was equal to *ca.* $24.83 \text{ cm}^3 \text{Kmol}^{-1}$ corresponding to the calculated value of $24.45 \text{ cm}^3 \text{Kmol}^{-1}$ for two uncoupled Er^{III} ($^4\text{I}_{15/2}$, $S = 3/2$, $L = 6$, $J = 15/2$, $g = 6/5$) and four uncoupled Cu^{II} ions ($S = 1/2$, $g = 2$). As shown in Figure 12, this value decreased with the lowering of the temperature to $13.93 \text{ cm}^3 \text{Kmol}^{-1}$ at 1.8 K.

The lowering of $\chi_M T$ at low temperature in 1 and 3, is caused most probably by the crystal field splitting of Ln^{III} ion, and/or a combination of the contribution of the overall antiferromagnetic interactions of metal ions. The profile of the $\chi_M T$ vs T curve in 2 strongly suggests the existence of two competitive phenomena. The decrease of $\chi_M T$ on temperature lowering was most probably caused by the depopulation of the Ho Stark sublevels, or the presence of magnetic anisotropy, or the antiferromagnetic coupling between ions, whereas, the increase of the $\chi_M T$ at lower temperatures may arise because of the ferromagnetic $\text{Cu}^{\text{II}}\text{-Ho}^{\text{III}}$ interaction.

4. Conclusions

The nuclearity of the presented complexes 1–3 was tuned by the interplay between coordination and hydrogen bonds involving nitrate anions. The recurrent array of coordination or semi-coordination bonds and hydrogen bonding presented here can be added to the crystal engineering library as a building motif. The coordination bond may be weakened and elongated until it transforms into a non-covalent interaction when a competitive influence of hydrogen bonding will occur. It is worth to underline that even at long distances (above the limit of semi-coordination bond 3.07 \AA) the directionality of the $\text{Cu} \cdots \text{O}-\text{NO}_2$ contact ($100\text{--}150^\circ$) may be sustained up to *ca.* 3.65 \AA , which also correlates well with the reports of Nelyubina et al. about weak but still attractive in nature interactions ($\text{Cu} \cdots \text{O} 3.6 \text{ \AA}$, 0.5 kcal/mol), which was involved in the magnetic super-exchange [34]. These may be regarded as crystallographic criteria for the searching of elongated semi-coordination bonds when

assisted by hydrogen bonding. On the basis of these results, the following conclusions can be drawn: That depending on the supramolecular topology and symmetry of the analyzed system, the hydrogen bonding can stabilize the coordination, or it can disrupt it. It seems that the stabilizing effect on semi-coordination bonding is observed when the accompanying hydrogen bond is directed to the non-coordinated O nitrate atom (see sets of contacts in crystal **3**: O3–H3···O19 and Cu2···O18; bifurcated O11–H11···O19/O20 and Cu4···O20). The destabilizing effect occurs when coordination and hydrogen bonding compete for the same O atom (see the pairs of contacts in **1**: O13–H13···O11 and Cu2···O11; in **2**: O8–H8···O35 and Cu1···O35; O4–H4···O26 and Cu2···O26). Additionally, the border of 3.07 Å for a semi-coordination bond can be probably extended when the “hydrogen bond assisted” coordination occurs, but additional angular preference factor must be considered.

The presented results show that hydrogen bonding has a significant influence on the coordination bonds being responsible for the weakening and the elongation of the axial out of plane bonds in structures disturbed by the Jahn–Teller effect. Irrespective of the semi-coordination bond distance limit, topological analysis of crystal structures should always be performed since even minor structural features may help in better understanding of physicochemical properties of coordination compounds, as well as in designing of self-assembling materials or in protein–ligand docking methods.

Supplementary Materials: The following are available online: <http://www.mdpi.com/2073-8994/11/4/460/s1>, **Figure S1.** Scatter plot of Cu···O–X(O₂) angle where X = C or N (ANG1 in °) vs Cu···O distance (CUO in Å) up to 4 Å with marked six regions described in the text; **Figure S2.** FTIR spectra of the **H₄tehy** ligand and complex **1**; **Figure S3.** FTIR spectra of the **H₄tehy** ligand and complex **2**; **Figure S4.** FTIR spectra of the **H₄tehy** ligand and complex **3**; **Figure S5.** TG and DSC curves of **1** in air; **Figure S6.** TG and DSC curves of **2** in air; **Figure S7.** TG and DSC curves of **3** in air; **Figure S8.** The powder XRD diffractograms of the final products of decomposition in air of complexes **1–3**.

Author Contributions: Conceptualization, B.M.; funding acquisition, B.M.; investigation, B.M., D.O., B.C., H.G.; methodology, B.M., B.C.; software, B.M.; visualization, B.M., D.O., B.C.; writing—original draft preparation, B.M., B.C.; writing—review and editing, B.M., B.C.

Funding: The research was carried out with the equipment purchased thanks to the financial support of the European Regional Development Fund in the framework of the Operational Program Development of Eastern Poland 2007–2013 (Contract No. POPW.01.03.00-06-009/11-00, equipping the laboratories of the Faculties of Biology and Biotechnology, Mathematics, Physics and Informatics, and Chemistry for studies of biologically active substances and environmental samples).

Acknowledgments: We kindly thank Prof. Keiji Hirose for the invitation to participate in this special issue on Symmetry and Asymmetry in Host-Guest Chemistry and Supramolecular Chemistry.

Conflicts of Interest: The authors declare no conflict of interest.

References

1. Sundberg, M.R. Effect of hydrogen bonding on coordinate bond. Semi-coordination in Werner-type copper(II) complexes revisited. *Rev. Inorg. Chem.* **2000**, *20*, 195–218. [[CrossRef](#)]
2. Grabowski, S.; Grabowski, J.S. Analysis of Hydrogen Bonds in Crystals. *Crystals* **2016**, *6*, 59. [[CrossRef](#)]
3. Videnova-Adrabińska, V. The hydrogen bond as a design element in crystal engineering. Two- and three-dimensional building blocks of crystal architecture. *J. Mol. Struct.* **1996**, *374*, 199–222.
4. Aakeröy, C.B.; Seddon, K.R. The hydrogen bond and crystal engineering. *Chem. Soc. Rev.* **1993**, *22*, 397–407. [[CrossRef](#)]
5. Desiraju, G.R. Reflections on the Hydrogen Bond in Crystal Engineering. *Cryst. Growth Des.* **2011**, *11*, 896–898. [[CrossRef](#)]
6. Etter, M.C.; MacDonald, J.C.; Bernstein, J. Graph-set analysis of hydrogen-bond patterns in organic crystals. *Acta Crystallogr. Sect. B Struct. Sci.* **1990**, *46*, 256–262. [[CrossRef](#)]
7. Miroslaw, B.; Koziol, A.E.; Bielenica, A.; Dziuba, K.; Struga, M. Substituent effect on supramolecular motifs in series of succinimide polycyclic keto derivatives—Spectroscopic, theoretical and crystallographic studies. *J. Mol. Struct.* **2014**, *1074*, 695–702. [[CrossRef](#)]
8. Ding, X.; Tuikka, M.; Haukk, M. Halogen Bonding in Crystal Engineering. In *Recent Advances in Crystallography*; Benedict, J.B., Ed.; IntechOpen: London, UK, 2012.

9. Mirosław, B.; Plech, T.; Wujec, M. Halogen bonding in the antibacterial 1,2,4-triazole-3-thione derivative - Spectroscopic properties, crystal structure and conformational analysis. *J. Mol. Struct.* **2015**, *1083*, 187–193. [[CrossRef](#)]
10. Mukherjee, A.; Tothadi, S.; Desiraju, G.R. Halogen Bonds in Crystal Engineering: Like Hydrogen Bonds yet Different. *Acc. Chem. Res.* **2014**, *47*, 2514–2524. [[CrossRef](#)]
11. Struga, M.; Mirosław, B.; Pakosinska-Parys, M.; Drzewiecka, A.; Borowski, P.; Kossakowski, J.; Koziol, A.E. Synthesis, characterization and supramolecular synthons in crystals of new derivatives of 10-oxa-4-azatricyclo[5.2.1.0^{2,6}]dec-8-ene-3,5-dione. *J. Mol. Struct.* **2010**, *965*. [[CrossRef](#)]
12. Madura, I.D.; Czerwińska, K.; Jakubczyk, M.; Pawełko, A.; Adamczyk-Woźniak, A.; Sporzyński, A. Weak C–H···O and Dipole–Dipole Interactions as Driving Forces in Crystals of Fluorosubstituted Phenylboronic Catechol Esters. *Cryst. Growth Des.* **2013**, *13*, 5344–5352. [[CrossRef](#)]
13. Desiraju, G.R.; Sarma, J.A.R.P.; Krishna, T.S.R. Dipole-dipole interactions and the inversion motif in the crystal structures of planar chloro aromatics: The unusual packings of 1,2,3-trichlorobenzene and 1,2,3,7,8,9-hexachlorodibenzo-p-dioxin. *Chem. Phys. Lett.* **1986**, *131*, 124–128. [[CrossRef](#)]
14. Newman, W.D.; Cortes, C.L.; Afshar, A.; Cadien, K.; Meldrum, A.; Fedosejevs, R.; Jacob, Z. Observation of long-range dipole-dipole interactions in hyperbolic metamaterials. *Sci. Adv.* **2018**, *4*, eaar5278. [[CrossRef](#)] [[PubMed](#)]
15. Mahmoudi, G.; Bauzá, A.; Gurbanov, A.V.; Zubkov, F.I.; Maniukiewicz, W.; Rodríguez-Diéguez, A.; López-Torres, E.; Frontera, A. The role of unconventional stacking interactions in the supramolecular assemblies of Hg(ii) coordination compounds. *CrystEngComm* **2016**, *18*, 9056–9066. [[CrossRef](#)]
16. Mahmoudi, G.; Zareba, J.K.; Bauzá, A.; Kubicki, M.; Bartyzel, A.; Keramidis, A.D.; Butusov, L.; Mirosław, B.; Frontera, A. Recurrent supramolecular motifs in discrete complexes and coordination polymers based on mercury halides: prevalence of chelate ring stacking and substituent effects. *CrystEngComm* **2018**, *20*, 1065–1076. [[CrossRef](#)]
17. James, S. Pi-Pi-Stacking as a Crystal Engineering Tool. In *Encyclopedia of Supramolecular Chemistry*; Atwood, J.L., Steed, J.W., Eds.; Marcel Dekker Inc.: New York, NY, USA, 2004; pp. 1093–1099.
18. Yao, Z.-F.; Wang, J.-Y.; Pei, J. Control of π - π Stacking via Crystal Engineering in Organic Conjugated Small Molecule Crystals. *Cryst. Growth Des.* **2018**, *18*, 7–15. [[CrossRef](#)]
19. Okuniewski, A.; Rosiak, D.; Chojnacki, J.; Becker, B. Coordination polymers and molecular structures among complexes of mercury(II) halides with selected 1-benzoylthioureas. *Polyhedron* **2015**, *90*, 47–57. [[CrossRef](#)]
20. Blagojević Filipović, J.P.; Hall, M.B.; Zarić, S.D. Stacking interaction potential energy surfaces of square-planar metal complexes containing chelate rings. *Adv. Inorg. Chem.* **2019**, *73*, 159–186.
21. Mahmudov, K.T.; Kopylovich, M.N.; Guedes da Silva, M.F.C.; Pombeiro, A.J.L. Non-covalent interactions in the synthesis of coordination compounds: Recent advances. *Coord. Chem. Rev.* **2017**, *345*, 54–72. [[CrossRef](#)]
22. Doyle, R.P.; Julve, M.; Lloret, F.; Nieuwenhuyzen, M.; Kruger, P.E. Hydrogen-bond tuning of ferromagnetic interactions: synthesis, structure and magnetic properties of polynuclear copper(ii) complexes incorporating p-block oxo-anions. *Dalt. Trans.* **2006**, *0*, 2081–2088. [[CrossRef](#)]
23. Tang, J.; Costa, J.S.; Golobic, A.; Kozlevcar, B.; Robertazzi, A.; Vargiu, A.V.; Gamez, P.; Reedijk, J. Magnetic coupling between copper(II) ions mediated by hydrogen-bonded (neutral) water molecules. *Inorg. Chem.* **2009**, *48*, 5473–5479. [[CrossRef](#)] [[PubMed](#)]
24. Mobin, S.M.; Srivastava, A.K.; Mathur, P.; Lahiri, G.K. Varying structural motifs in oxyanions (NO₃⁻, CO₃²⁻) and phenoxyacetate (PhOAc⁻) bridged coordination polymers derived from alkoxo-bridged dicopper building blocks with {Cu₂O₂} core. *RSC Adv.* **2011**, *1*, 893–902. [[CrossRef](#)]
25. Haldar, S.; Vijaykumar, G.; Carrella, L.; Musie, G.T.; Bera, M. Structure and properties of a novel staircase-like decanuclear [Cu^{II}₁₀] cluster supported by carbonate and carboxylate bridges. *New J. Chem.* **2018**, *42*, 1276–1283. [[CrossRef](#)]
26. Takeda, S.; Watanabe, A.; Maruta, G.; Matsuo, T. Magnetic Interactions through Short Hydrogen Bond in Hydrogen-Bonded Basic Copper (II) Salt; Cu 2 Na(D 3 O 2)(SO 4) 2. *Mol. Cryst. Liq. Cryst.* **2002**, *376*, 443–448. [[CrossRef](#)]
27. Brown, D.S.; Lee, J.D.; Melsom, B.G.A.; Hathaway, B.J.; Procter, I.M.; Tomlinson, A.A.G. The structure of Cu(en)₂(BF₄)₂ and an infrared spectral criterion for “semi-co-ordinated” polyanions. *Chem. Commun. (London)* **1967**, *0*, 369–371. [[CrossRef](#)]

28. Valach, F. A bond-valence approach to the semicoordination of copper-oxygen and copper-nitrogen complexes. *Polyhedron* **1999**, *18*, 699–706. [[CrossRef](#)]
29. Valach, F.; Rohlíček, J.; Lukeš, V.; Kožíšek, J.; Jorík, V. Manifestation of copper coordination sphere plasticity in $[\text{Cu}_2(2\text{-bromopropionato})_4]_n$ and $[\text{Cu}_2(3\text{-bromopropionato})_4(\text{H}_2\text{O})_2]$. *Inorganica Chim. Acta* **2018**, *479*, 106–112. [[CrossRef](#)]
30. Choi, J.-H.; Joshi, T.; Spiccia, L. Syntheses, Structural, and Spectroscopic Properties of Copper(II) Complexes of Constrained Macrocyclic Ligands. *Zeitschrift für Anorg. und Allg. Chemie* **2012**, *638*, 146–151. [[CrossRef](#)]
31. Bikbaeva, Z.M.; Ivanov, D.M.; Novikov, A.S.; Ananyev, I.V.; Bokach, N.A.; Kukushkin, V.Y. Electrophilic–Nucleophilic Dualism of Nickel(II) toward Ni···I Noncovalent Interactions: Semicoordination of Iodine Centers via Electron Belt and Halogen Bonding via σ -Hole. *Inorg. Chem.* **2017**, *56*, 13562–13578. [[CrossRef](#)]
32. Valach, F.; Grobelny, R.; Glowiak, T.; Mrozinski, J.; Lukeš, V.; Blahová, Z. Structural study of semi-coordination in a seven-coordinate copper(II) complex: distortion isomerism of $[\text{Cu}(\text{CH}_3\text{COO})_2(4\text{-aminopyridine})_2(\text{H}_2\text{O})]$. *J. Coord. Chem.* **2010**, *63*, 1645–1651. [[CrossRef](#)]
33. Nimmermark, A.; Öhrström, L.; Reedijk, J. Metal-ligand bond lengths and strengths: are they correlated? A detailed CSD analysis. *Zeitschrift für Krist. - Cryst. Mater.* **2013**, *228*, 311–317. [[CrossRef](#)]
34. Nelyubina, Y.V.; Korlyukov, A.A.; Fedyanin, I.V.; Lyssenko, K.A. Extremely long Cu···O contact as a possible pathway for magnetic interactions in $\text{Na}_2\text{Cu}(\text{CO}_3)_2$. *Inorg. Chem.* **2013**, *52*, 14355–14363. [[CrossRef](#)]
35. Brunsveld, L.; Folmer, B.J.B.; Meijer, E.W.; Sijbesma, R.P. Supramolecular Polymers. *Chem. Rev.* **2001**, *101*, 4071–4098. [[CrossRef](#)] [[PubMed](#)]
36. Winter, A.; Hager, M.D.; Schubert, U.S. Supramolecular Polymers. *Polym. Sci. A Compr. Ref.* **2012**, 269–310.
37. De Greef, T.F.A.; Smulders, M.M.J.; Wolfs, M.; Schenning, A.P.H.J.; Sijbesma, R.P.; Meijer, E.W. Supramolecular Polymerization. *Chem. Rev.* **2009**, *109*, 5687–5754. [[CrossRef](#)] [[PubMed](#)]
38. Krieg, E.; Bastings, M.M.C.; Besenius, P.; Rybtchinski, B. Supramolecular Polymers in Aqueous Media. *Chem. Rev.* **2016**, *116*, 2414–2477. [[CrossRef](#)] [[PubMed](#)]
39. Cristóvão, B.; Mirosław, B.; Bartyzel, A. Hexanuclear $[\text{Cu}_4^{\text{II}}\text{Ln}_2^{\text{III}}]$ compounds incorporating N,O-donor ligands—Synthesis, crystal structures and physicochemical properties. *Inorganica Chim. Acta* **2017**, *466*, 160–165. [[CrossRef](#)]
40. Cristóvão, B.; Osypiuk, D.; Mirosław, B.; Bartyzel, A. Syntheses, crystal structures, thermal and magnetic properties of new heterotrinary $\text{Cu}^{\text{II}}\text{-Ln}^{\text{III}}\text{-Cu}^{\text{II}}$ complexes incorporating N_2O_4 -donor Schiff base ligands. *Polyhedron* **2018**, *144*, 225–233. [[CrossRef](#)]
41. Bermejo, M.R.; Fernández, M.I.; Gómez-Fórneas, E.; González-Noya, A.; Maneiro, M.; Pedrido, R.; Rodríguez, M.J. Self-Assembly of Dimeric MnIII–Schiff-Base Complexes Tuned by Perchlorate Anions. *Eur. J. Inorg. Chem.* **2007**, *2007*, 3789–3797. [[CrossRef](#)]
42. Aguiari, A.; Bullita, E.; Casellato, U.; Guerriero, P.; Tamburini, S.; Vigato, P.A. Macrocyclic and macroacyclic compartmental Schiff bases: synthesis, characterization, X-ray structure and interaction with metal ions. *Inorganica Chim. Acta* **1992**, *202*, 157–171. [[CrossRef](#)]
43. Kahn, O. *Molecular Magnetism*; VCH Publishers, Inc.: New York, NY, USA, 1993.
44. Rigaku Oxford Diffraction Ltd. *Crysalis-Pro Software System*; ver. 1.171.38.46; Rigaku Corporation Ltd.: Oxford, UK, 2016.
45. Sheldrick, G.M. Crystal structure refinement with SHELXL. *Acta Crystallogr. Sect. C Struct. Chem.* **2015**, *71*, 3–8. [[CrossRef](#)]
46. Dolomanov, O.V.; Bourhis, L.J.; Gildea, R.J.; Howard, J.A.K.; Puschmann, H. OLEX2: A complete structure solution, refinement and analysis program. *J. Appl. Crystallogr.* **2009**, *42*, 339–341. [[CrossRef](#)]
47. Bruno, I.J.; Cole, J.C.; Edgington, P.R.; Kessler, M.; Macrae, C.F.; McCabe, P.; Pearson, J.; Taylor, R. IUCr New software for searching the Cambridge Structural Database and visualizing crystal structures. *Acta Crystallogr. Sect. B Struct. Sci.* **2002**, *58*, 389–397. [[CrossRef](#)]
48. Brandenburg, K.; Putz, H. *Diamond*; Crystal Impact GbR: Bonn, Germany, 2006.
49. Li, G.-B.; Hong, X.-J.; Gu, Z.-G.; Zheng, Z.-P.; Wu, Y.-Y.; Jia, H.-Y.; Liu, J.; Cai, Y.-P. Efficient synthesis and characterization of the low dimensional heteronuclear complexes with a N_2O_2 -donor Schiff base ligand. *Inorganica Chim. Acta* **2012**, *392*, 177–183. [[CrossRef](#)]

50. Alaghaz, A.-N.M.A.; El-Sayed, B.A.; El-Henawy, A.A.; Ammar, R.A.A. Synthesis, spectroscopic characterization, potentiometric studies, cytotoxic studies and molecular docking studies of DNA binding of transition metal complexes with 1,1-diaminopropane–Schiff base. *J. Mol. Struct.* **2013**, *1035*, 83–93. [[CrossRef](#)]
51. Dubey, R.K.; Baranwal, P.; Jha, A.K. Zinc(II) and mercury(II) complexes with Schiff bases: syntheses, spectral, and structural characterization. *J. Coord. Chem.* **2012**, *65*, 2645–2656. [[CrossRef](#)]
52. Bartyzel, A. Synthesis, crystal structure and characterization of manganese(III) complex containing a tetradentate Schiff base. *J. Coord. Chem.* **2013**, *66*, 4292–4303. [[CrossRef](#)]
53. Gutiérrez, A.; Perpiñán, M.F.; Sánchez, A.E.; Torralba, M.C.; González, V. Water inclusion mediated structural diversity and the role of H-bonds in molecular assemblies of manganese(III) bicompartamental Schiff-base complexes. *Inorganica Chim. Acta* **2016**, *453*, 169–178. [[CrossRef](#)]



© 2019 by the authors. Licensee MDPI, Basel, Switzerland. This article is an open access article distributed under the terms and conditions of the Creative Commons Attribution (CC BY) license (<http://creativecommons.org/licenses/by/4.0/>).